Ahuir-Torres, JI, Chadwick, J, West, G, Kotadia, HR and Opoz, TT

Effect of electrical discharge machining (EDM) bath composition on long-term corrosion of Ti-6Al-4V in simulated body fluid

Electrochimica Acta 503 (2024) 144865

Contents lists available at ScienceDirect

Electrochimica Acta

journal homepage: www.journals.elsevier.com/electrochimica-acta

Effect of electrical discharge machining (EDM) bath composition on long-term corrosion of Ti-6Al-4V in simulated body fluid

J.I. Ahuir-Torres [a,*], J. Chadwick [b], G. West [c], H.R. Kotadia [b,c], T.T. Öpöz [a]

[a] General Engineering Research Institute, School of Engineering, Faculty of Engineering and Technology, Liverpool John Moores University, Byrom Street, Liverpool, L3 3AF, UK
[b] School of Engineering, Faculty of Engineering and Technology, Liverpool John Moores University, Byrom Street, Liverpool, L3 3AF, UK
[c] WMG, University of Warwick, Coventry, CV4 7AL, UK

ARTICLE INFO

Keywords:
Ti-6Al-4V
Electrical discharge machining
Corrosion
Simulated body fluid
Electrochemical impedance spectroscopy

ABSTRACT

Ti-6Al-4V (Ti64) alloy is a widely used bioimplant material due to its excellent properties. However, long-term exposure to body fluids can lead to corrosion, a concern given increasing lifespans. Electrical discharge machining (EDM) can improve Ti64 corrosion resistance at long term. This study investigates the long-term corrosion behaviour of Ti64 in simulated body fluid (SBF) after EDM treatment using different bath compositions (oil, water, and hydroxyapatite dissolution (HA)). Electrochemical and microscopy techniques were used to analyse corrosion mechanisms over immersion periods ranging from 2 h to 3 months. Results show that EDM-treated samples in water exhibited the highest corrosion resistance, while those processed in oil possessed the lowest. Especially, the corrosion resistance of samples treated in water and HA remained constant over time, unlike the non-EDMed and oil-treated samples. Furthermore, all samples exhibited evolving corrosion mechanisms over time, with faster deposition of SBF elements observed on oil and HA-treated samples, suggesting enhanced biointegration potential. The thicker deposited SBF layer on these samples further supports the potential of these EDM treatments to improve the biointegration of Ti64 implants.

1. Introduction

Ti-6Al-4V (Ti64) finds wide application in various bioimplants, including dental, hip, and knee replacements. Ti64 acceptance stems from its excellent properties, such as high corrosion resistance and favourable bone integration (osseointegration) [1–5]. However, with increasing life expectancies, there is a growing need to extend bioimplant lifespans for several decades. The harsh environment of body fluids and internal temperatures can corrode Ti alloys over the long term [1,4,6]. This corrosion compromises the integrity of the Ti64 implant and its bond with the bone, potentially leading to failure. Fluorine ions found in saliva can deteriorate dental implants by dissolving the protective Ti oxide layer [5,7]. Similarly, blood anions (e.g., chlorine, sulphate, carbonate, and phosphate) can damage this passive film, inducing corrosion [4,6,8]. Human body temperature (≈37.5 °C) further accelerates this dissolution process [4,9]. Beyond implant failure, Ti64 corrosion releases potentially harmful alloying elements: V, which is cytotoxic, and Al, which has been linked to Alzheimer's disease [3,10]. Therefore, improving the corrosion resistance of Ti64 is crucial for its continued advancement in bioimplant applications.

Various techniques can enhance the corrosion resistance of Ti alloys, including anodising [11,12], plasma electrolytic oxidation [13], ion implantation [14], sol-gel coatings [15], laser alloying [2] and laser selective melting [16] and electrical discharge machining (EDM) [1, 17–20]. EDM, in particular, stands out due to its ability to machine high-strength and low-conductivity materials. As a non-contact process, EDM utilizes controlled electrical sparks to erode the surface, enabling complex shapes, precise dimensions, and good finishes. Furthermore, its low-temperature nature minimises thermal damage to the Ti, crucial for bioimplant applications. Particularly, EDM can also improve biocompatibility and promote desired surface topography, enhancing hydrophilicity (cell adhesion), proliferation, and anchorage of bone cells [21–26].

EDM is a non-traditional machining process that utilises electrical sparks within a dielectric fluid to melt and vaporise (removal) material from the workpiece [27,28]. While highly effective for hard-to-cut materials such as Ti, the intense heat and specific dielectric fluid can influence the corrosion behaviour of the machined surface. Parameters

* Corresponding author.
E-mail address: j.i.ahuirtorres@ljmu.ac.uk (J.I. Ahuir-Torres).

https://doi.org/10.1016/j.electacta.2024.144865
Received 11 April 2024; Received in revised form 28 July 2024; Accepted 6 August 2024
Available online 8 August 2024

such as spark energy, discharge frequency, and dielectric fluid type play a crucial role in balancing efficient material removal with desired surface integrity and corrosion resistance [29]. Appropriate control of these parameters is essential to minimise thermal damage, reduce the formation of undesirable surface oxides, and ensure the longevity of the machined component in potentially corrosive environments [30,31].

EDM enhances Ti alloy corrosion resistance by creating layers with low chemical activity and strong substrate adhesion [1]. The specific layer characteristics depend on the EDM bath. In low-aggression environments, EDM induces microstructural changes that yield a new, highly corrosion-resistant layer [20]. For water baths (aggressive environments), EDM thickens the native passive film for greater protection [19]. Particularly, EDM with hydroxyapatite (HA) solution baths can deposit a well-compacted, strongly adherent HA layer on the substrate. This also offers further protection against harsh environments [1,18]. Crucially, even with imperfections, EDM-produced oxide layers effectively increase corrosion resistance in both water and HA baths. Oil baths can lead to the formation of heterogeneous TiC layers, promoting galvanic corrosion and reducing corrosion resistance compared to untreated samples. Conversely, aggressive environments like deionised water and HA baths encourage the formation of protective oxide layers, enhancing corrosion resistance. Additionally, EDM capacitance plays a crucial role, as excessive capacitance can induce cracks in the oxide layer, while insufficient capacitance may hinder its formation, both negatively impacting corrosion resistance [32].

While existing research has explored the short-term corrosion resistance of EDMed Ti64 [32], the long-term behaviour and the influence of different EDM bath types remain understudied. This study aims to address this gap by investigating the corrosion resistance of Ti64 machined using EDM with three distinct baths: oil, distilled water (water), and a HA solution in distilled water (HA). The surface morphology and cross-sections have been examined using scanning electron microscopy and the chemical composition has been assessed with energy dispersive spectroscopy. The electrochemical impedance spectroscopy (EIS) employed to analyse the corrosion resistance and mechanisms of the samples over long immersion times in simulated body fluid (SBF), providing valuable insights for bioimplant applications.

2. Experimental methods

2.1. Materials and EDM experiments

A rectangular Ti-6Al-4V Grade 5 sheet (55 mm × 80 mm with 3 mm thickness) served as the workpiece material for EDM machining. Experiments were conducted on a Hurco 50A Mark 2 die sinking EDM machine using a 6 mm solid graphite electrode. Three dielectric fluids were investigated: EDM oil, deionised water, and a 10 g/L HA (particle sizes ranging from 10 to 15 μm, supplied by Medicoat SAS based in France) mixture in deionised water. A digital mixer ensured continuous agitation and prevented HA particle sedimentation during machining. The EDM capacitance was set to 10 nF, resulting in varying average pulse currents based on the bath (0.61 A for water, 0.83 A for HA water, 1.06 A for oil). A summary of the experimental conditions is presented in Table 1. Each test condition was repeated three times for a total of nine EDMed surfaces (three per bath) for corrosion analysis. The experimental setup is illustrated in Fig. 1 and representative images of the machined surfaces are presented in Fig. 2.

2.2. Electrochemical analyses

EDMed samples were used as received, while non-EDMed samples were polished with P1200 silicon carbide abrasive paper. Samples were cleaned with detergent, rinsed with water, and finally cleaned with isopropanol before testing. The chemical composition of SBF is detailed in Table 2, and is closely resembles those employed in previous research [6,12,33,34]. The chemical agent used were supplied by Merck-Sigma-Aldrich. The pH was adjusted using a pH metre (Jenway 350 pH metre supplied by Scientific Laboratory Supplies) and maintained at 37.5 °C with a hot plate (Stuart, SB162 provided by BioCote).

Table 1
Key parameters and settings for the EDM experiment.

Parameter	Description
EDM machine	Hurco 50A Mark 2
Workpiece	Ti6Al4V (Ti64)
Electrode	Solid circular graphite (6 mm in dia.)
Dielectric fluid	• Fully Synthetic Dielectric Oil (Corsmot EDM/CH PLUS) • Deionised water, • Hydroxyapatite (HA) mixed in deionised water (10 g/L HA concentration)
Pulse time (μs)	20
Duty cycle (%)	50
Capacitance (nF)	10
Polarity (electrode)	Negative

The electrochemical tests were carried out with a potentio/galvanostat (Interface1010E) from Gamry Instruments Inc. A potentiostat/galvanostat was used with Gamry software for data acquisition and analysis. The three-electrode cell was employed on electrochemical trials. The reference electrode was silver/silver chloride in 3 M KCl (Ag/AgCl 3 M KCl) with double junction (EDT direct ion limited). The counter electrode was a platinum wire with 0.7 mm diameter (Cooksonglod Heimerle + Meule Group). The working electrodes were the samples. The electrochemical impedance spectroscopy (EIS) testing was used for the corrosion analysis. The tests were conducted with 10 mV potential amplitude in root mean square, a frequency range from 10^{-2} Hz to 10^{5} Hz and 10 points per frequency decade.

To assess corrosion evolution, EIS was conducted at various immersion times (2 to 2352 h (14 weeks)). Equivalent circuit method was used to analyse the obtained data with Gamry software. Each test was repeated at least three times to check results consistency.

To ensure consistent SBF ion concentrations throughout the testing period, samples were capped with plastic film between measurements to minimise evaporation. In the rare event of slight volume loss, distilled water was added (two to three times) to restore the original SBF volume, carefully avoiding any significant changes in concentration.

2.3. Surface and microstructure analysis

The EDM surfaces were analysed before and after the corrosion process using various microscopy techniques. To assess surface topography and roughness, a Bruker Contour GT-K 3D (Bruker) white light interferometer equipped with Vision 64 software (optical light profilometer) was used. The average areal surface roughness (Sa) values were used to compare the surface roughness of EDM surfaces under different dielectric fluid conditions and capacitance settings. Scanning Electron Microscopy (SEM) with Energy Dispersive Spectroscopy (EDS) was employed to analyse the surface characteristics and chemical composition of the samples. The SEM analysis was conducted at 10 kV with a beam current of 8.0 nA, a spot size of 2.0, secondary and backscattered electrons. Standard Buehler grinding methods were used to prepare the samples for SEM analysis. This was followed by polishing with a finishing grit of 0.05 μm. After polishing, a vibratory polisher with a silica suspension liquid (VibroMet™) was used for a two-hour treatment.

3. Results and discussion

3.1. EDMed surface and microstructure analysis

Fig. 3 shows the average surface roughness (Sa) of EDMed and non-EDMed surfaces under different bath conditions. Surfaces machined in oil have the highest roughness (Sa = 3.68 μm) due to larger crater

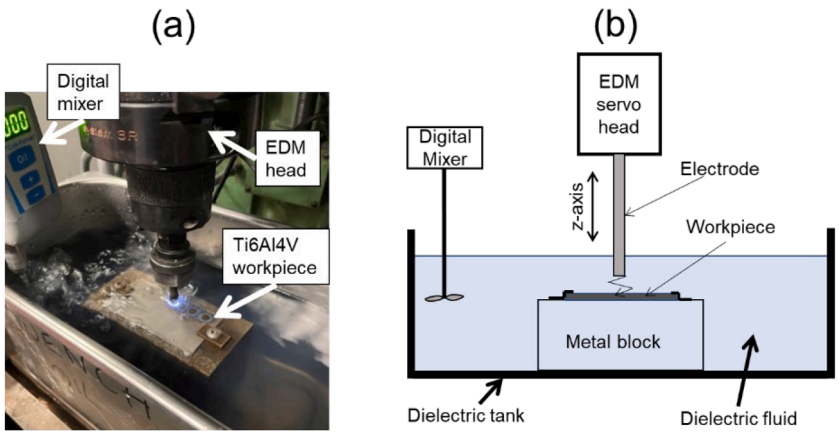

Fig. 1. EDM experiment set-up: (a) photograph and (b) schematic diagram illustrating the key components of the EDM setup.

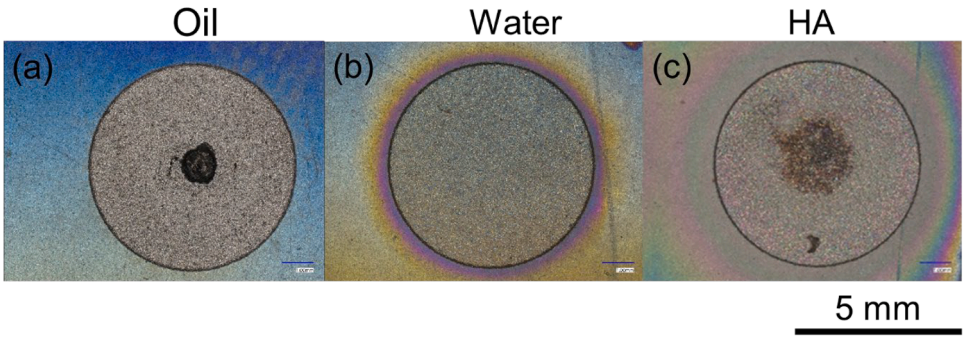

Fig. 2. Representative examples of surfaces (Keyence VHX series digital optical light microscopy picture) created by EDM in (a) oil, (b) deionised water, and (c) a mixture of HA in deionised water baths.

Table 2
Chemical composition of SBF in g/L [6,12,33,34].

Chemical compound	Quantity (g/L distilled water)
NaCl	8.035
$NaHCO_3$	0.355
KCl	0.225
$K_2HPO_4{\cdot}3H_2O$	0.231
$MgCl_2.H_2O$	0.311
$CaCl_2.H_2O$	0.292
Na_2SO_4	0.072
$(CH_2OH)_3(CNH_2)$	6.118
pH	7.400

formations. Conversely, surfaces treated in deionised water (Sa = 3.23 μm) and especially those machined with HA-mixed deionised water (Sa = 2.55 μm) exhibit significantly lower roughness with smaller craters, contributing to smoother overall topographies. Particularly, HA-mixed deionised water also demonstrates superior repeatability, with a lower standard deviation (0.151) compared to oil (0.809) and deionised water (1.021).

SEM analyses (Fig. 3) of top view of the EDMed sample reveals more pronounced crack formation on surfaces treated with deionised water compared to those machined in oil. This observation aligns with the roughness data and suggests a connection between crack formation and surface morphology. Furthermore, surfaces treated with HA-mixed deionised water exhibit less crack formation, further supporting the beneficial effects of this bath composition.

Cutting fluids significantly influence crack formation and morphology in Ti machining. Fig. 4 focuses on the cross-section of the EDMed surfaces, their features relevant to corrosion analysis. While crack formation is evident in both deionised water and HA-mixed deionised water baths, it appears less prevalent in oil-treated surfaces. Interestingly, the deionised water bath also leads to a thicker white layer compared to the oil bath. Oil-based fluids offer lubrication but hinder chip evacuation, promoting microcracks along grain boundaries [28,35]. Water-based fluids provide excellent cooling but poor lubrication, potentially leading to larger, interconnected cracks due to increased stress and possible hydrogen embrittlement [28]. HA fluids can act as a solid lubricant and form a protective coating [21], potentially reducing crack formation, but may introduce stress concentrations under specific conditions. Furthermore, localized melting during EDM can result in an uneven surface, a heat-affected zone (HAZ), and residual stresses, all of which vary in morphology depending on the specific dielectric fluid used [36].

Figs. 5 and 6 present the chemical composition of the sample from a side view, assessed via EDS mapping (Fig. 5) and element concentration as a function of depth (Fig. 6). Additionally, carbide formation (TiC) is observed on oil-treated surfaces (Fig. 5**(b)** and Fig. 6**(b)**), while oxide formation is present on deionised water-treated surfaces (water (Fig. 5 **(c)** and Fig. 6**(c)**) and HA (Fig. 5**(c)** and Fig. 6**(c)**)). These observations regarding the white layer and potential carbide/oxide formation will be further addressed in the corrosion analysis section to understand their impact on corrosion resistance.

3.2. *Electrochemical analyses*

Fig. 7 shows the evolution of corrosion mechanisms over time for the samples, as visualised by Nyquist (imaginary vs. real impedance) and Bode plots (phase angle and impedance modulus vs. frequency). These results were used to identify six equivalent circuits representing the various corrosion mechanisms (Fig. 8). These plots are used for comparing corrosion behaviours of different samples with respect to

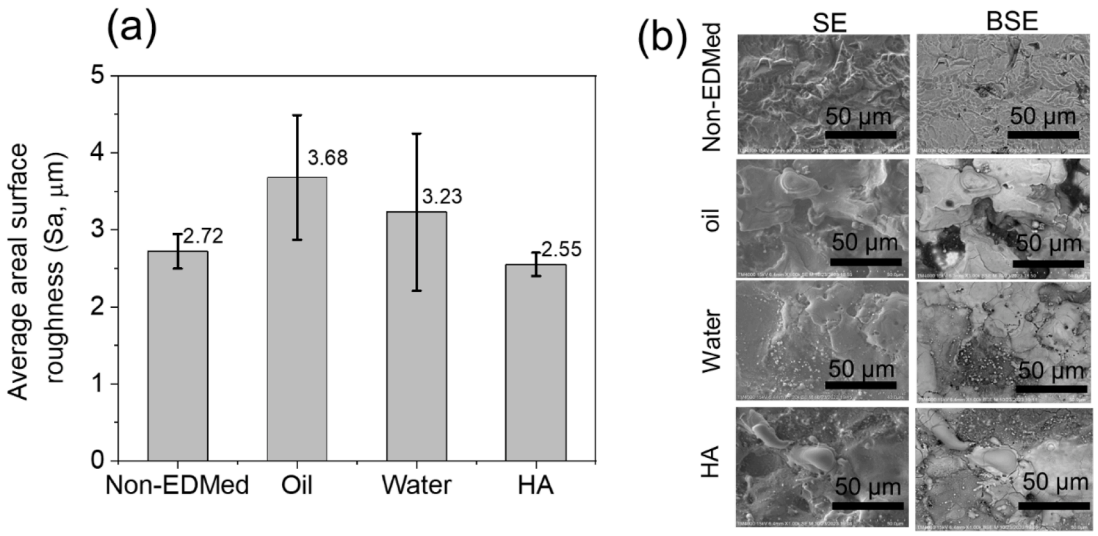

Fig. 3. (a) Averaged areal surface roughness (Sa) and (b) topographic SEM images (Secondary Electron (SE) and Backscatter Electron (BSE)) of the surfaces treated by EDM under various dielectric bath conditions.

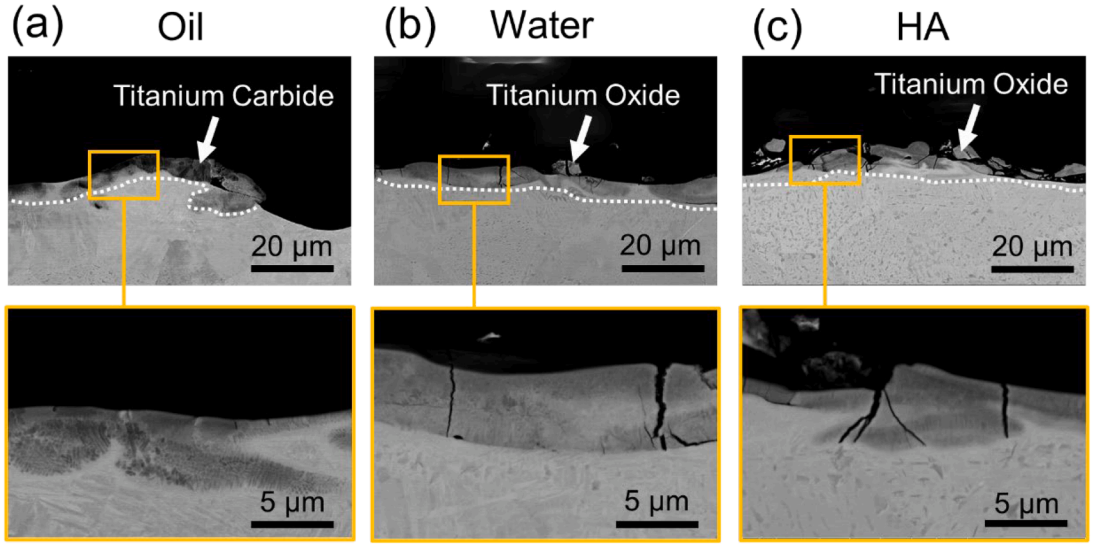

Fig. 4. SEM images with backscattered electrons, illustrating the (a) oil, (b) water, and (c) HA EDM samples in a section view.

immersion time.

First equivalent circuit (Fig. 8**(a)**): This circuit consists of three-time constants. The first is represented by a horizontal curve in the Z_{mod} vs. F plot at 10^5 Hz, indicating a resistance (R_1) [37]. The second is a constant phase element (CPE_2) due to its horizontal curve in the θ vs. F plot from 10^{-2} Hz to 10^{-1} Hz, a slope change in the Z_{mod} vs. F plot at the same frequencies, and a tail at the highest real impedance in the Nyquist plot [38]. The third time constant comprises of a constant phase element (CPE_3) in parallel with a resistance (R_3), evident by an inclined curve in the Z_{mod} vs. F plot from 10^{-1} Hz to 10^3 Hz, an inclined curve followed by a peak in the θ vs. F plot for the same range, and a positive loop in the Nyquist plot [39]. These elements are connected in series, with R_3 parallel with CPE_2 and both in series with R_1. This circuit is commonly used in similar studies [32].

Second equivalent circuit (Fig. 8**(b)**): This circuit shares the same elements as the first but adds an extra resistance (R_2) in the second time constant, reflected by the curve inclination at 10^{-2} Hz in the θ vs. F plot and the flattening of the loop in the Nyquist plot [40]. This resistance can also manifest as two peaks in the θ vs. F plot and an additional loop in the Nyquist plot due to the low overlap between the second- and third-time constants [40]. R_2 is connected in parallel with CPE_2. This circuit has been used by researchers to model the corrosion behaviour of Ti64 in body fluid [38,40,41].

Third equivalent circuit (Fig. 8**(c)**): This circuit builds upon the second by adding another constant phase element (CPE_4) in parallel with an additional resistance (R_4). This is identified by an extra peak in the θ vs. F plot, a slope changes in the Z_{mod} vs. F plot, and another loop in the Nyquist plot, all observed between 10^2 Hz and 10^3 Hz for Bode plots [34]. CPE_4 is connected in parallel with R_4 and in series with R_3.

Fourth equivalent circuit (Fig. 8**(d)**): This circuit includes five-time constants, with the first four resembling the previous circuit. The fifth time constant is similar to the others, consisting of a constant phase element (CPE_5) in parallel with a resistance (R_5) and connected in series with R_4. Similar signals are observed in the Bode and Nyquist plots compared to the previous circuit, but at higher frequencies (10^3 Hz to 10^4 Hz for Bode and medium real impedance for Nyquist).

Fifth equivalent circuit (Fig. 8**(e)**): This circuit resembles the third but incorporates an inductor as the fifth time constant. This element is connected in series with R_1 and R_2 and in parallel with CPE_3. Its presence is indicated by the negative loop at the lowest real impedance in the

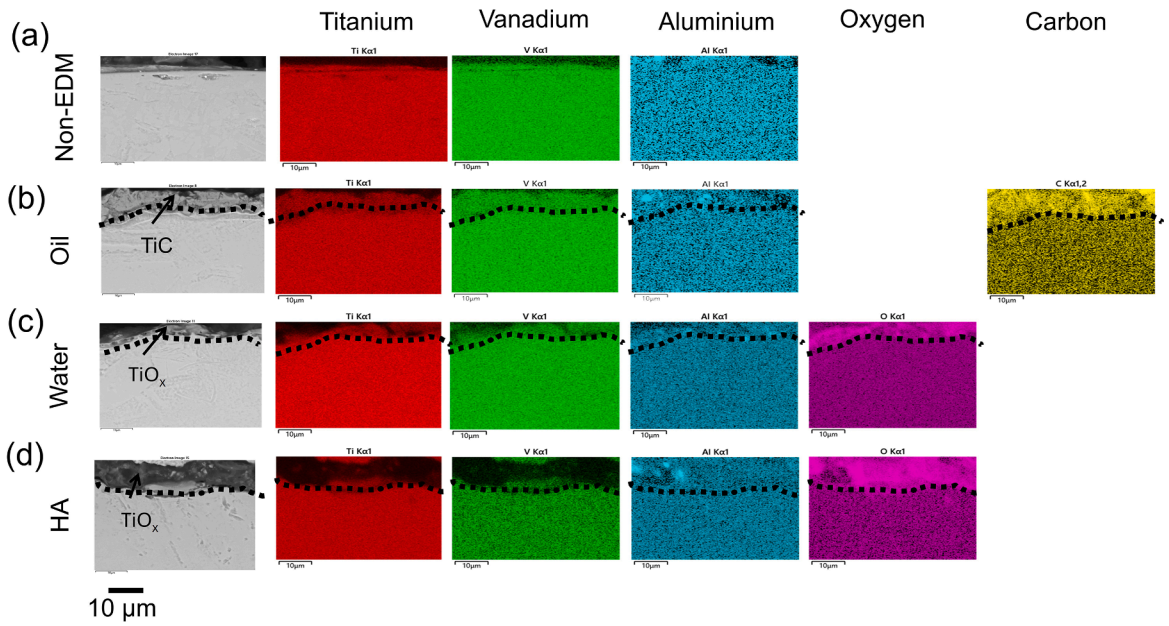

Fig. 5. Cross-sectional EDS elemental mapping images with backscattered electrons of (a) non-EDMed, (b) oil EDMed, (c) water EDMed, and (d) HA EDMed Ti64 samples.

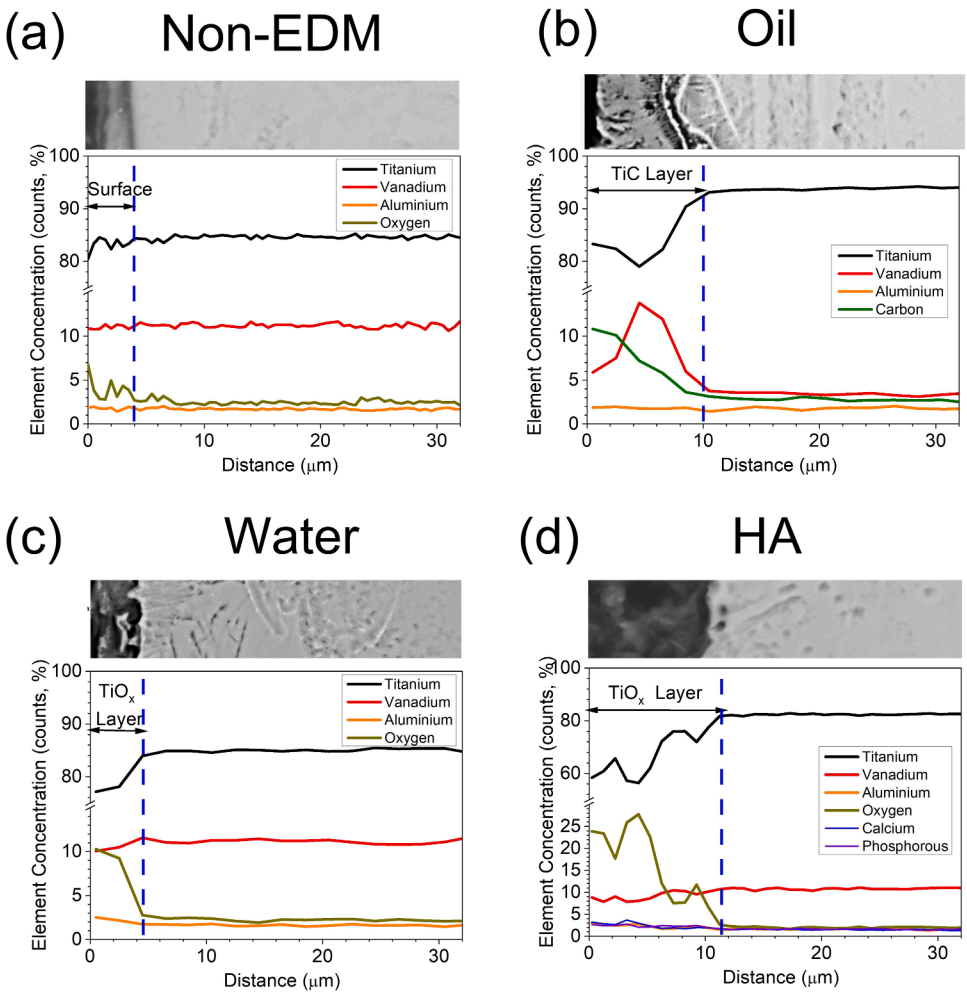

Fig. 6. Depth-dependant EDS analysis (with backscattered electrons) of (a) non-EDMed, (b) oil EDMed, (c) water EDMed, and (d) HA EDMed Ti64 samples.

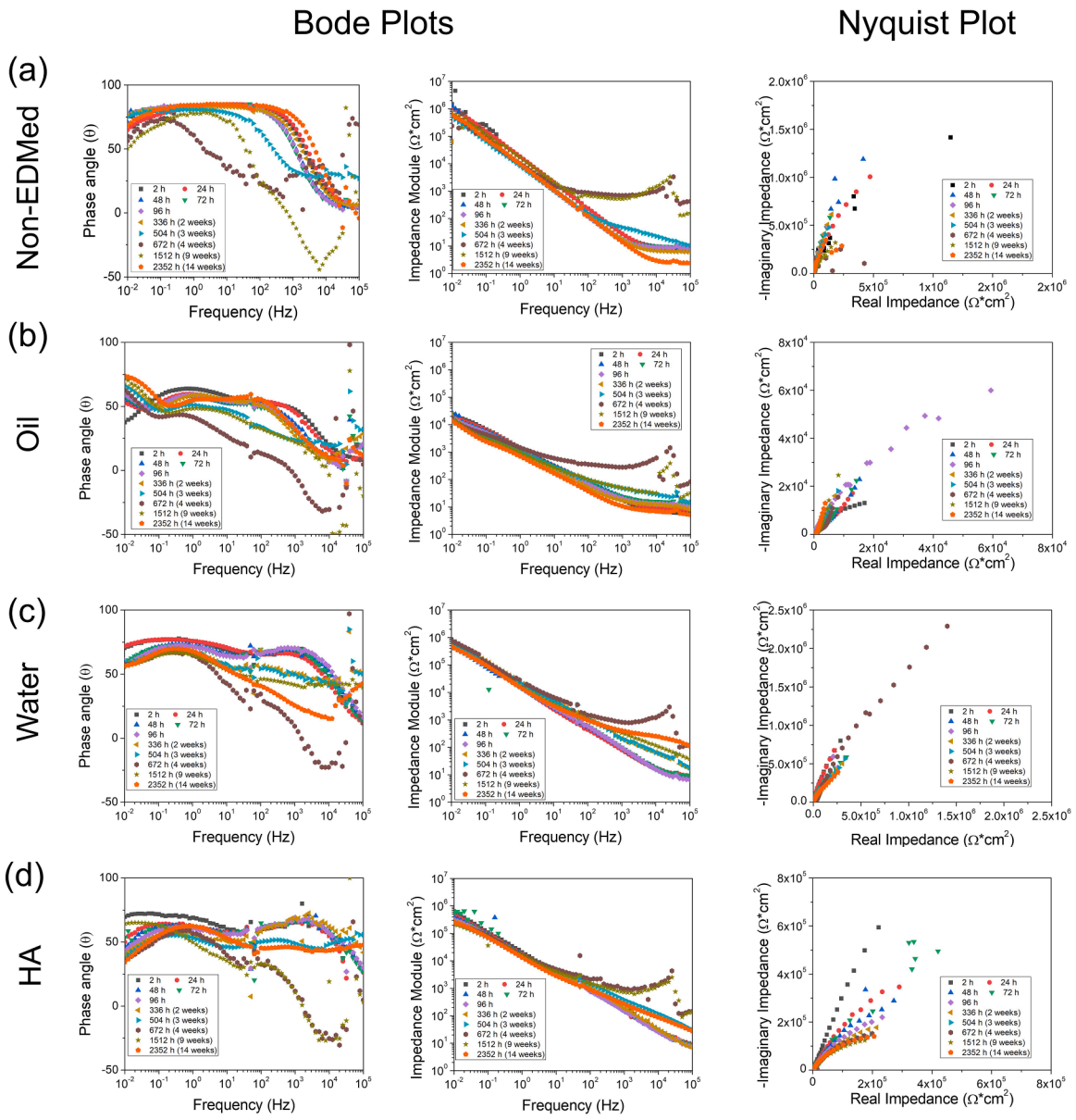

Fig. 7. EIS data (10 nF) for (a) non-EDMed and EDMed Ti64 samples ((b) oil, (c) water, (d) HA baths) immersed in SBF (pH 7.4, 37.5 °C) for durations ranging from 2 h to 2352 h (14 weeks).

Nyquist plot and the negatively sloped curve in the Bode plots between 10^4 Hz and 10^5 Hz. Inductors are associated with adsorption-desorption processes [42–45].

Sixth equivalent circuit (Fig. 8**(f)**): This final circuit includes a Warburg impedance element alongside the components from the previous circuit. This element manifests as a tail at high real impedance in the Nyquist plot and at 10^{-2} Hz for both Bode plots. Warburg impedance is linked to diffusion processes [38,42,46].

The corrosion mechanisms of the samples varied based on their immersion time in the SBF, as evidenced by the distinct equivalent circuits listed in Table 3. This observation, where different circuits were needed for the same samples at different immersion times, indicates an evolution of the corrosion mechanisms over time [6,32].

The equivalent circuits used to model the corrosion mechanisms were validated by the strong agreement between experimental EIS data (Fig. 9) and low chi-squared values (Tables 4). Circuit element evolution varied significantly across sample types.

R_1 remained near 10 Ωcm^2 for all samples before increasing and then decreasing over time. The increase occurred around 672 h for most samples, except HA-EDMed (1512 h). Resistance values ranked as follows: Water-EDMed > HA-EDMed > Non-EDMed > Oil-EDMed.

The evolution of the second time constant differed between samples. For non-EDMed samples, R_2 remained constant ($M\Omega cm^2$), while CPE_2 decreased, suggesting thinning of the corrosion process [47]. n_2 was initially stable (≈0.9) then decreased (≈0.82), indicating increased surface roughness [48]. For oil-EDMed samples, values were consistent across immersion times with exceptions at the beginning (lower R_2) and end (higher R_2), potentially indicating increased resistance without thickening. n_2 decreased, suggesting continuous degradation with some recovery at the end [49,50]. In HA-EDMed samples, CPE_2 was constant ($\approx \mu S s^{-n} cm^{-2}$), and R_2 increased up to 336 h ($\approx M\Omega cm^2$) before decreasing, suggesting changes in resistance without a change in thickness. n_2 decreased and then increased, indicating increased roughness followed by smoothing. For water-EDMed samples, CPE_2 remained constant ($\mu S s^{-n} cm^{-2}$), R_2 increased, and n_2 fluctuated slightly, implying increased resistance without affecting thickness or surface quality [4].

The third time constant also exhibited sample-specific evolution. It

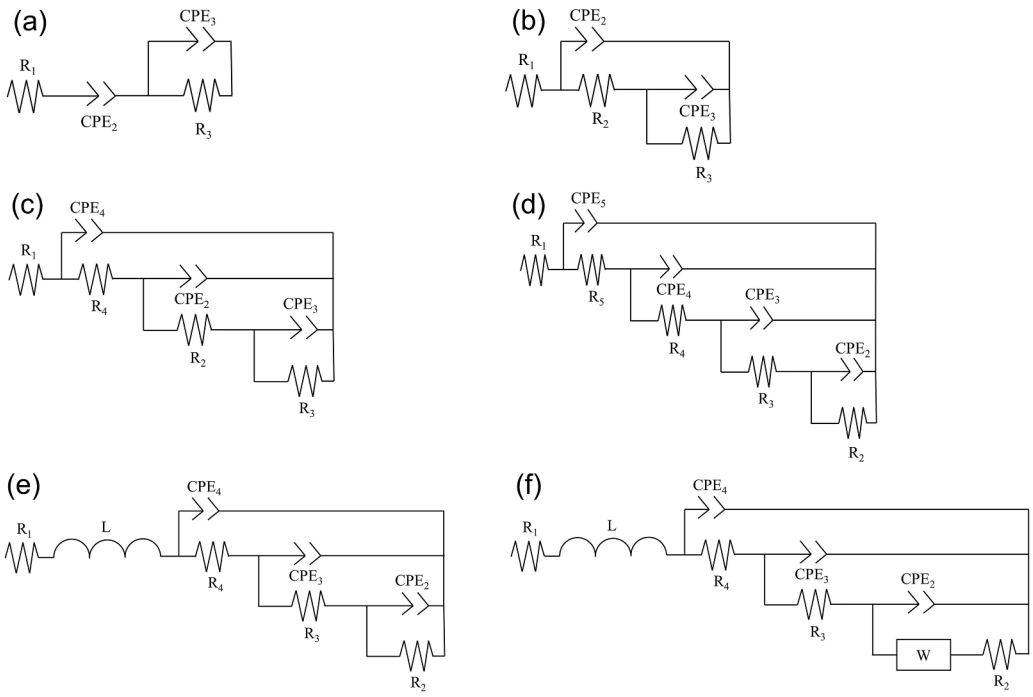

Fig. 8. Equivalent circuits used to model the corrosion mechanisms of the samples at different immersion times: (a) first, (b) second, (c) third, (d) fourth, (e) fifth, and (f) sixth.

Table 3
Summary of the equivalent circuit associated to each sample and immersion time.

Immersion Time (h)	Type of Equivalent Circuit			
	Non-EDMed	Oil EDMed	HA EDMed	Water EDMed
2	Second	Second	First	First
24	Second	Second	Second	Second
48	Second	Third	Second	Second
72	Second	Fourth	Third	Second
96	Second	Fourth	Third	Second
336	Second	Fourth	Third	Third
504	Third	Fourth	Third	Third
672	Fifth	Sixth	Fifth	Fifth
1512	Fifth	Sixth	Fifth	Third
2352	Third	Fourth	Third	Fourth

fluctuated for most samples, indicating instability [51]. The exception was water-EDMed, where elements remained constant (R_3 at $M\Omega cm^2$, CPE_3 at $\mu Ss^{-n}cm^{-2}$, and n_3 around 0.7–1.0), suggesting a highly stable process [52].

The fourth time constant appeared later for some samples (non-EDMed ≥ 504 h, oil-EDMed ≥ 48 h, HA-EDMed ≥ 72 h, water-EDMed at 336 h). Trends varied across samples, with non-EDMed showing increased R_4 and decreased CPE_4 (thickening with increased resistance [4,34]), oil-EDMed showing correlated CPE_4 and R_4 behaviour (thinning with increased resistance due to compaction [6,34]), HA-EDMed showing decreased R4 (reduced resistance with constant thickness and surface quality), and water-EDMed exhibiting fluctuations implying a dynamic process [51].

Induction (L) appeared at 672 and 1512 h for most samples (except water-EDMed, only at 672 h). Most had inductances of tens $mHcm^{-2}$, with oil-EDMed being the exception with lower values (units of mH/cm^2).

A fifth time constant emerged only in non-EDMed samples (at 72, 504, and 2352 h) and for oil-EDMed (at 2352 h). Generally, in non-EDMed samples, R5 decreased over time, indicating reduced resistance, while CPE_5 and n_5 remained mostly constant. Notably, at 2352 h, higher R_5, n_5 approaching 0.9, and similar CPE_5 implied a smoothing of the corrosion process surface [5,34] and increased resistance without thickening [53].

Finally, Warburg impedance appeared only in oil-EDMed samples (at 672 and 1512 h) and decreased over time, indicating a reduction in diffusion processes [38].

3.3. Microstructure analysis after electrochemical test

After 2352 h of immersion, the sample surfaces exhibited numerous imperfections, including cracks and pitting (Fig. 10). This damage likely arises from the localised dissolution of the native passive film, TiC layer, and EDMed oxidised layer by anions (e.g., Cl^-, SO_4^{-2}, and CO_3^{-2}) present in the solution [4]. The depth of the damage, revealing the internal microstructure in non-EDM (Fig. 10**(a)**) and oil-EDMed (Fig. 10**(b)**) specimens, suggests a severe breakdown of the passive layer and reduced corrosion resistance. The presence of bright (BSE), round particles on all sample surfaces, likely composed of cations and ions from the SBF, indicates heterogeneous salt deposition. These deposits can be composed of calcium cations and phosphate anions, which are known to adhere to Ti64 alloy surfaces [17,48]. EDS mapping of the surface (Fig. 11) confirmed the chemical composition and the presence of a deposited SBF layer. The heterogeneous nature of this layer was evident from the micro-spherical clusters composed of Ca, Al, O, C, and P observed on the surface of all samples.

SEM with BE revealed a deposited layer on the surface of all samples (Fig. 12). This deposition is likely the result of SBF cations and ions interacting with the surface at high temperatures (37.5 °C) over the extended immersion period [17,48]. Cross-sectional analysis showed an absence of deep, new cracks within the samples, suggesting that the observed corrosion damage is primarily confined to the surface.

EDS analysis confirmed SBF salt deposition on the specimen surfaces, as evidenced by the presence of O and Ca within the top layer (Figs. 13 and 14). This deposited layer also contained Ti and alloying elements (Al and V), suggesting its integration with the underlying substrate. The heterogeneous and discontinuous nature of the layer's chemical composition indicated variations in salt deposition between specimens.

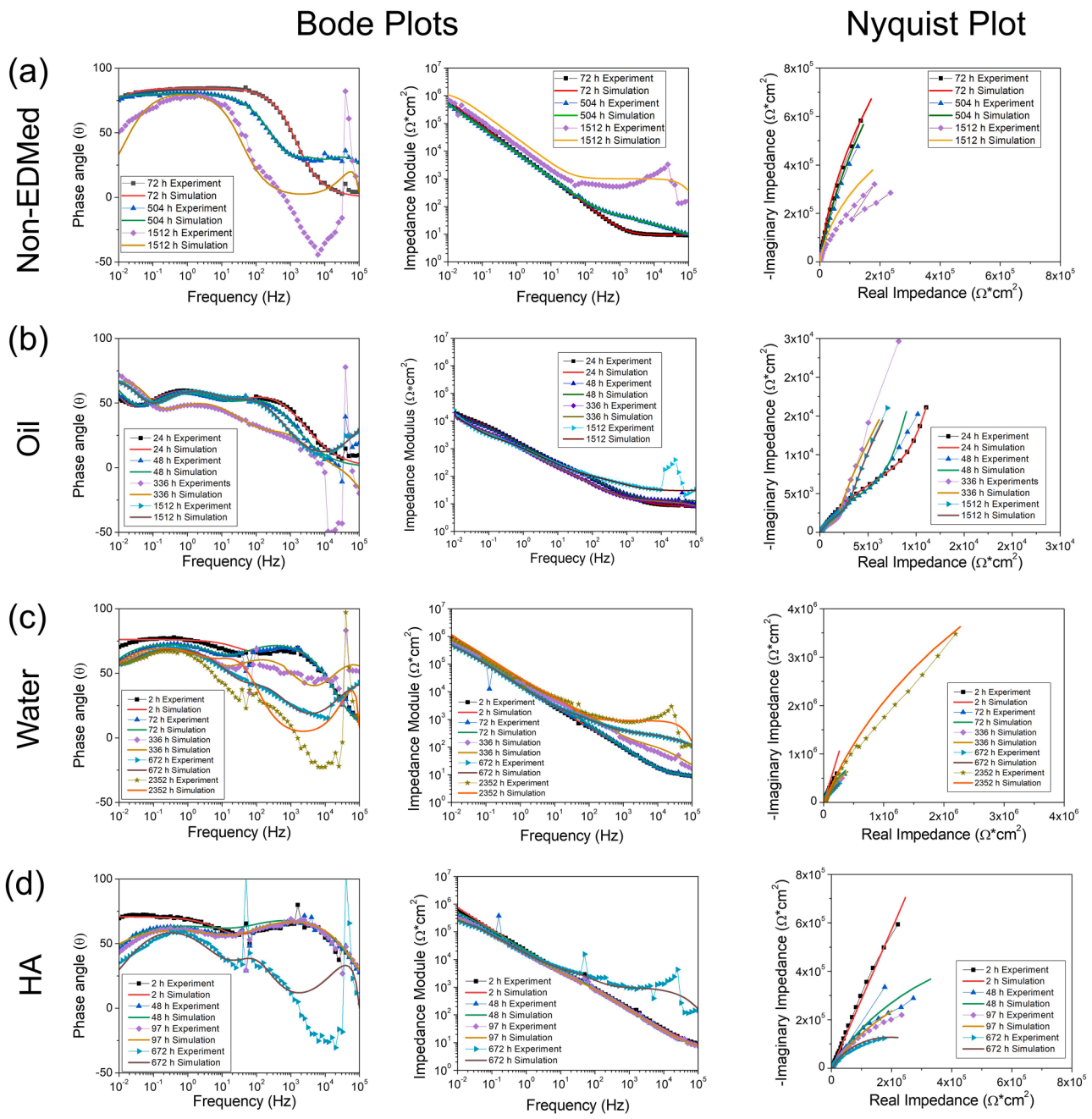

Fig. 9. Experimental and simulated EIS data for (a) non-EDMed and EDMed Ti6Al4V immersed in (b) oil, (c) distilled water, and (d) hydroxyapatite dissolution (HA) in SBF (pH 7.4, 37.5 °C). Samples were compared across different immersion times, with changes in the equivalent circuit analysed for each individual sample.

Element concentrations generally followed the order: EDMed with oil (Figs. 13**(b)** and 14**(b)**) ≈ EDMed with HA (Figs. 13**(d)** and 14**(d)**) > EDMed with water (Figs. 13**(c)** and 14**(c)**) > Non-EDMed (Figs. 13**(a)** and 14**(a)**). This suggests that the initial deposited layers may have a higher salt concentration. High surface roughness and suitable surface chemistry likely accelerate salt deposition [15,54,55]. Notably, beneath the deposited layer, the concentrations of Ti64 elements were reduced in localized areas, accompanied by the presence of O. This indicates substrate oxidation beneath the deposited layer, likely facilitated by imperfections (pores and cracks) that allow oxygen access to the Ti64 surface [15].

The absence of cytotoxic V and potentially harmful Al in the deposited SBF layer of HA-EDMed samples is a notable finding, suggesting reduced risk of adverse effects and enhanced biocompatibility compared to other EDM treatments [3,10]. While Al was detected in other samples, its absence in HA-EDMed samples may offer further benefits in terms of long-term safety. This highlights the potential of HA-EDM treatment to minimize the release of potentially harmful ions, making it a promising approach for improving the biocompatibility of Ti implants.

3.4. Corrosion evolution over the time assessment

Controlled EDM experiments, correlated with detailed characterisation and electrochemical EIS analysis, have revealed distinct differences in the corrosion behaviour of Ti64 alloy samples. This study demonstrates that both the EDM bath composition and the formation of surface layers significantly influence the way corrosion evolves over time in SBF. Electrochemical analysis findings were further corroborated by a post-corrosion microstructure analysis, which aided in the identification

Table 4
Values of the equivalent circuit elements for non-EDMed, oil, Ha and water EDMed samples according to the immersion time in SBF.

Time (h)	R_1 (Ωcm^2)	R_2 (Ωcm^2)	CPE_2 (Ss^n/cm^{-2})	n_2	R_3 (Ωcm^2)	CPE_3 (Ss^n/cm^{-2})	n_3	R_4 (Ωcm^2)	CPE_4 (Ss^n/cm^2)	n_4	R_5 (Ωcm^2)	CPE_5 (Ss^n/cm^{-2})	n_5	W ($Stcm^{-2}$)	t ($s^{1/2}$)	L (H/cm^2)	X^2 (10^{-4})
Non-EDMed sample																	
2	8.76	1.10×10^6	1.96×10^{-5}	0.94	2.21×10^2	1.19×10^{-3}	0.86	–	–	–	–	–	–	–	–	–	9.12
24	10.02	1.68×10^6	2.05×10^{-5}	0.93	3.10×10^2	1.33×10^{-3}	0.86	–	–	–	–	–	–	–	–	–	7.49
48	8.17	9.01×10^5	1.94×10^{-5}	0.94	2.60×10^6	2.43×10^{-6}	0.80	–	–	–	–	–	–	–	–	–	8.39
72	9.41	4.72×10^5	1.87×10^{-5}	0.94	1.30×10^6	5.27×10^{-7}	0.95	–	–	–	–	–	–	–	–	–	11.20
96	8.57	1.09×10^6	1.93×10^{-5}	0.94	6.41×10^7	1.59×10^{-5}	0.90	–	–	–	–	–	–	–	–	–	3.18
336	6.14	3.25×10^6	2.04×10^{-5}	0.92	5.52×10^2	3.44×10^{-7}	0.91	–	–	–	–	–	–	–	–	–	3.83
504	6.90	3.02×10^6	1.50×10^{-5}	0.90	2.34×10^1	3.12×10^{-6}	0.83	38.90	4.79×10^{-6}	0.92	–	–	–	–	–	–	7.25
672	118.44	9.35×10^6	1.07×10^{-5}	0.93	1.31×10^5	1.11×10^{-5}	0.86	127.00	3.33×10^{-9}	1.00	–	–	–	–	–	2.99×10^{-2}	391.00
1512	89.72	1.54×10^5	5.81×10^{-6}	0.94	1.28×10^6	7.11×10^{-7}	0.73	914.00	2.64×10^{-9}	1.00	–	–	–	–	–	3.99×10^{-2}	932.00
2352	2.47	2.82×10^6	6.72×10^{-6}	0.82	6.62×10^3	1.24×10^{-7}	1.00	166.00	1.21×10^{-5}	0.99	–	–	–	–	–	–	9.46
Oil EDMed Samples																	
2	5.53	2.11×10^2	6.72×10^{-3}	0.74	3.96×10^4	6.36×10^{-6}	0.71	–	–	–	–	–	–	–	–	–	10.70
24	7.76	4.38×10^2	1.05×10^{-4}	0.74	2.40×10^4	2.66×10^{-6}	0.96	–	–	–	–	–	–	–	–	–	7.30
48	12.62	1.89×10^4	1.18×10^{-4}	0.70	2.06×10^6	4.87×10^{-4}	0.97	404.00	9.51×10^{-5}	0.75	–	–	–	–	–	–	3.81
72	7.63	1.67×10^4	1.01×10^{-4}	0.71	2.36×10^6	2.10×10^{-6}	0.90	7.20	1.80×10^{-7}	0.99	4.93×10^2	1.26×10^{-4}	0.73	–	–	–	4.52
96	10.45	1.56×10^4	1.28×10^{-4}	0.70	1.38×10^5	5.08×10^{-4}	1.00	12.60	9.84×10^{-7}	0.78	3.09×10^2	1.05×10^{-4}	0.77	–	–	–	6.29
336	2.90	7.76×10^3	1.40×10^{-4}	0.73	1.67×10^5	4.71×10^{-4}	0.98	12.00	2.70×10^{-6}	0.76	2.75×10^2	1.29×10^{-4}	0.78	–	–	–	4.89
504	14.91	1.33×10^4	2.02×10^{-4}	0.63	2.67×10^8	2.79×10^{-4}	1.00	22.80	1.17×10^{-6}	0.78	8.91×10^1	8.74×10^{-5}	0.62	–	–	–	9.98
672	37.87	2.95×10^3	1.47×10^{-5}	0.61	8.89×10^3	4.74×10^{-5}	0.84	244.00	2.10×10^{-8}	1.00	–	–	–	2.84×10^{-2}	0.92	2.84×10^{-3}	512.00
1512	29.52	5.33×10^3	2.43×10^{-4}	0.65	8.12×10^4	3.38×10^{-4}	1.00	71.30	3.23×10^{-5}	0.79	–	–	–	3.00×10^{-3}	16.87	3.00×10^{-3}	60.30
2352	6.27	6.22×10^6	4.44×10^{-4}	0.96	4.40×10^5	4.61×10^{-3}	0.54	925.00	2.68×10^{-4}	0.73	2.80×10^3	9.70×10^{-5}	0.92	–	–	–	1.70
HA EDMed Samples																	
2	6.37	–	6.65×10^{-6}	0.78	4.18×10^3	5.17×10^{-6}	0.80	–	–	–	–	–	–	–	–	–	7.81
24	6.73	4.52×10^3	6.82×10^{-6}	0.78	5.42×10^6	8.88×10^{-6}	0.68	–	–	–	–	–	–	–	–	–	13.20
48	5.89	3.30×10^3	6.25×10^{-6}	0.79	2.08×10^6	1.08×10^{-5}	0.66	–	–	–	–	–	–	–	–	–	4.58
72	6.25	8.62×10^5	8.93×10^{-6}	0.72	1.72×10^7	1.97×10^{-2}	0.84	5380.00	7.19×10^{-6}	0.78	–	–	–	–	–	–	20.50
96	5.25	1.30×10^6	1.21×10^{-5}	0.65	4.74×10^5	2.47×10^{-4}	0.88	3350.00	6.77×10^{-6}	0.79	–	–	–	–	–	–	13.70

(*continued on next page*)

Table 4 (*continued*)

Time (h)	R_1 (Ωcm^2)	R_2 (Ωcm^2)	CPE_2 (Ss^n/cm^{-2})	n_2	R_3 (Ωcm^2)	CPE_3 (Ss^n/cm^{-2})	n_3	R_4 (Ωcm^2)	CPE_4 (Ss^n/cm^2)	n_4	R_5 (Ωcm^2)	CPE_5 (Ss^n/cm^{-2})	n_5	W ($Stcm^{-2}$)	t ($s^{1/2}$)	L (H/cm^2)	X^2 (10^{-4})
336	3.52	2.31×10^6	1.54×10^{-5}	0.64	9.62×10^5	2.02×10^{-9}	0.91	4100.00	4.83×10^{-6}	0.80	–	–	–	–	–	–	6.50
504	3.86	7.64×10^3	6.66×10^{-6}	0.66	5.26×10^6	1.11×10^{-5}	0.69	224.00	1.48×10^{-6}	0.75	–	–	–	–	–	–	1.40
672	77.78	3.33×10^3	1.74×10^{-6}	0.94	3.88×10^5	1.54×10^{-5}	0.73	990.00	1.21×10^{-7}	0.76	–	–	–	–	–	5.53×10^{-2}	420.00
1512	237.52	2.15×10^3	1.20×10^{-6}	1.00	2.83×10^6	1.67×10^{-5}	0.72	100.00	4.04×10^{-9}	1.00	–	–	–	–	–	7.89×10^{-2}	438.00
2352	6.31	2.08×10^3	7.45×10^{-6}	0.69	4.11×10^6	9.11×10^{-6}	0.78	147.00	2.42×10^{-6}	0.73	–	–	–	–	–	–	8.33
Water EDMed Samples																	
2	8.46	–	6.60×10^{-6}	0.84	1.89×10^3	2.94×10^{-6}	0.85	–	–	–	–	–	–	–	–	–	10.60
24	6.01	3.91×10^3	8.00×10^{-6}	0.82	3.15×10^6	4.64×10^{-6}	0.83	–	–	–	–	–	–	–	–	–	5.94
48	6.61	2.83×10^3	7.80×10^{-6}	0.83	3.90×10^6	5.78×10^{-6}	0.80	–	–	–	–	–	–	–	–	–	4.15
72	8.65	5.48×10^3	6.64×10^{-6}	0.84	6.98×10^6	5.14×10^{-6}	0.80	–	–	–	–	–	–	–	–	–	4.20
96	5.83	2.94×10^3	6.95×10^{-6}	0.84	8.72×10^7	6.74×10^{-6}	0.78	–	–	–	–	–	–	–	–	–	7.61
336	6.11	1.04×10^4	5.18×10^{-6}	0.77	3.23×10^6	4.95×10^{-6}	0.80	136.00	4.27×10^{-7}	0.87	–	–	–	–	–	–	31.70
504	5.44	1.18×10^4	6.75×10^{-6}	0.72	1.28×10^7	2.39×10^{-6}	0.89	94.80	1.32×10^{-6}	0.80	–	–	–	–	–	–	56.20
672	292.92	1.26×10^4	2.47×10^{-6}	0.96	4.48×10^6	5.37×10^{-6}	0.75	908.00	3.88×10^{-9}	1.00	–	–	–	–	–	3.21×10^{-2}	463.00
1512	15.51	4.54×10^3	6.61×10^{-6}	0.70	2.02×10^6	4.64×10^{-6}	0.85	322.00	3.39×10^{-6}	0.69	–	–	–	–	–	–	7.71
2352	28.15	1.24×10^6	7.66×10^{-6}	0.81	8.33×10^6	3.24×10^5	1.00	294.00	3.12×10^{-7}	0.77	2.31×10^3	6.55×10^{-6}	0.77	–	–	–	7.92

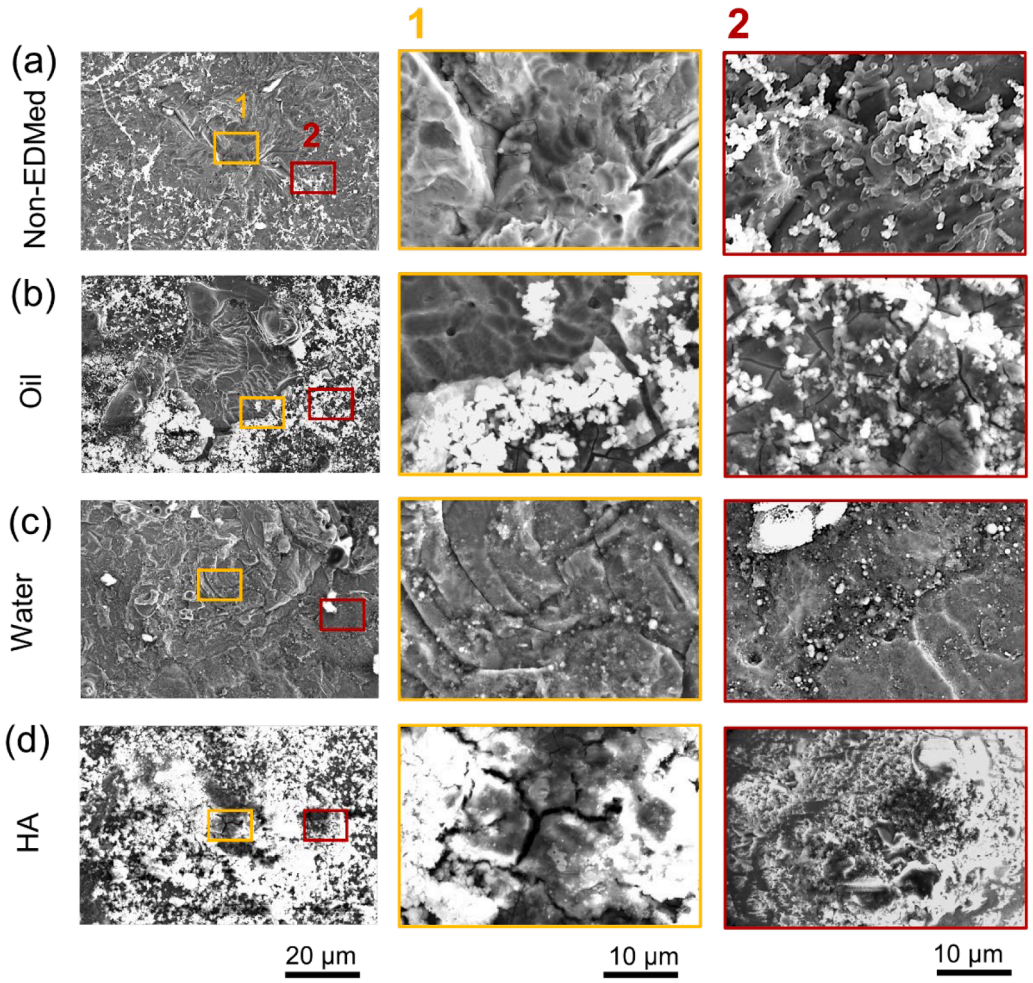

Fig. 10. SEM images (SE) showing surface damage on Ti64 samples after 2352 h in SBF (pH 7.4, 37.5 °C). (a) Non-EDMed, (b) oil-EDMed, (c) water-EDMed, (d) HA-EDMed.

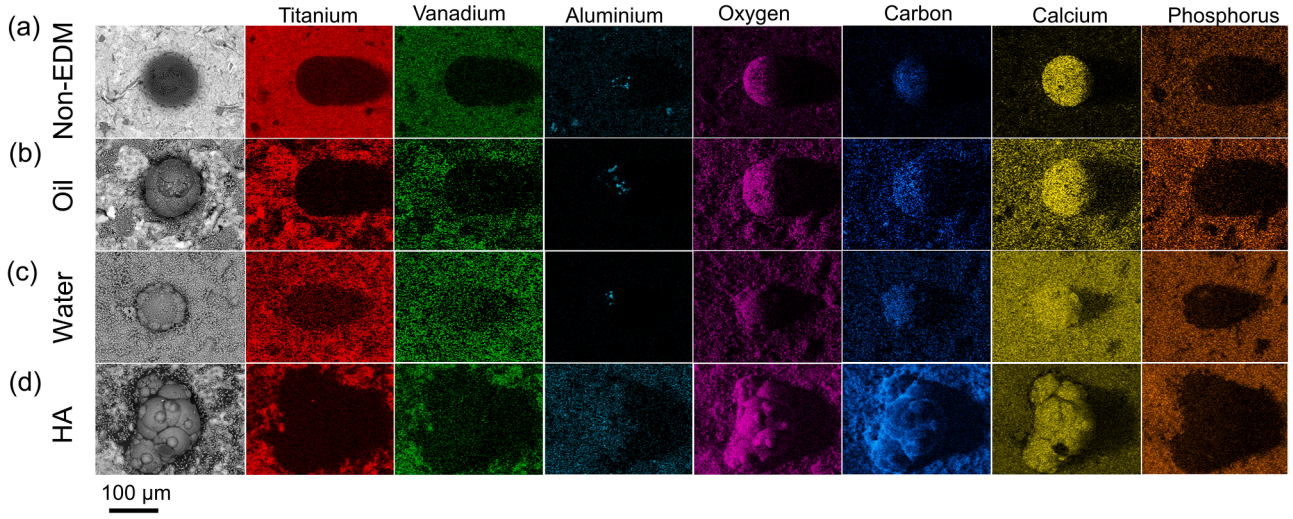

Fig. 11. EDS elemental mapping images of the sample surfaces after 2352 h of immersion in SBF (pH 7.4, 37.5 °C): (a) Non-EDMed, (b) oil-EDMed, (c) water-EDMed, (d) HA-EDMed.

and classification of various corrosion products formed on the surface. EIS analyses highlighted that, depending on the EDM treatment and subsequent immersion time, Ti64 samples exhibited dissimilar corrosion mechanisms.

EIS analysis revealed several time constants corresponding to distinct corrosion processes. Particularly, R_1 consistently represented the solution resistance (R_s) across all samples [40]. The second time constant was associated with the passive film for most samples, except for the

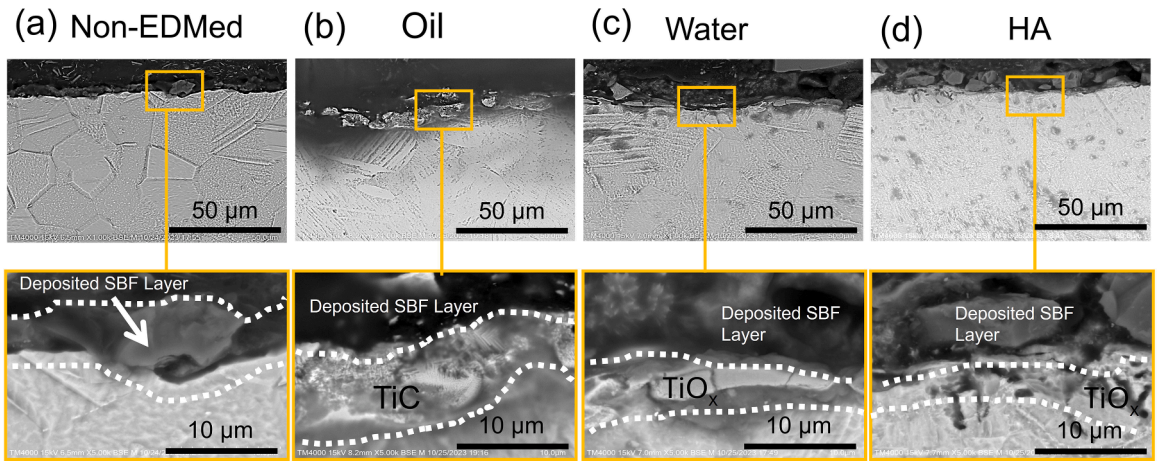

Fig. 12. SEM cross-section images (secondary electrons) revealing deposited SBF layers on Ti64 samples after 2352 h in SBF (pH 7.4, 37.5 °C). Treatments include: (a) Non-EDMed, (b) oil-EDMed, (c) water-EDMed, (d) HA-EDMed.

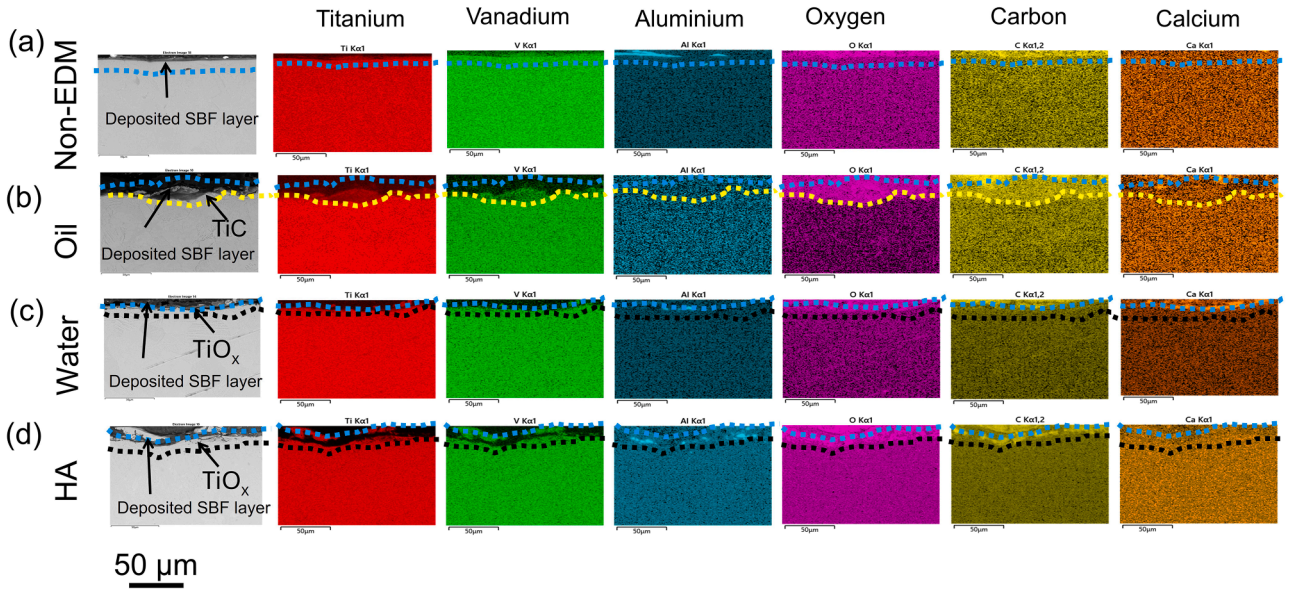

Fig. 13. Cross-sectional EDS elemental maps of Ti64 samples after 2352 h of immersion in SBF (pH 7.4, 37.5 °C): (a) Non-EDMed, (b) oil-EDMed, (c) water-EDMed, and (d) HA-EDMed.

oil-EDMed samples at the initial immersion times (2 and 24 h), where it related to the TiC layer [40]. This time constant encompassed the double layer capacitance (CPE_f) and exponent (n_f) alongside the charge transfer resistance (R_f) of the passive film [38,44,49,56]. The third time constant consistently represented the bare material for all samples, with CPE_3 (CPE_{dl}) reflecting the double layer capacitance associated with the charge separation process, and R_3 (R_{ct}) corresponding to the charge transfer resistance [38,44,49,56]. The inductior (L) and Warburg impedance (W) appeared in some samples, signifying the influence of adsorption-desorption processes on the deposited layer and the diffusion impedance arising from cracks and pores [38].

The fourth time constant, representing the dissolution of deposited elements, manifested in most samples, while the oil-EDM_{ed} samples exhibited it in the fifth time constant. This deposition likely arises due to the high temperature (37.5 °C) and long-term immersion, leading to the formation of an additional protective layer on the metallic surface [48]. The double layer capacitance (CPE_{de}) and exponent (n_{de}) along with the charge transfer resistance (R_{de}) within this time constant characterized the deposited layer. Interestingly, for the oil-EDMed samples, the fourth time constant specifically related to the TiC layer, denoted by CPE_{TiC}, n_{TiC}, and R_{TiC} [57]. This highlights the distinct protective properties of the TiC layer compared to the passive film. Finally, the fifth time constant in water-EDMed samples represented the sub-passive film, denoted by R_{sf}, CPE_{sf}, and n_{sf} [4]. This indicates the potential formation of a secondary passive layer beneath the primary one under specific conditions.

The corrosion mechanism evolution for each sample type is illustrated schematically in Fig. 15. Non-EDMed samples exhibited a four-stage evolution (Fig. 15**(a)**). Initially (2 to 336 h), the corrosion mechanism was characterised by passive film formation and bare material exposure [4]. The passive film thickness increased continuously over time. The second stage (504 h) introduced the deposition of dissolved SBF elements onto the sample surface, forming an additional protective layer [17]. Both the resistance and thickness of this layer increased with time, suggesting a correlation between corrosion resistance and layer thickness [4]. At the third stage (672 to 2352 h), an adsorption-desorption process involving water, O, and deposited elements was observed. This process, likely influenced by elements like magnesium [51] was absent in the final stage (2532 h) where the deposited layer thinned. This thinning could be due to re-dissolution or

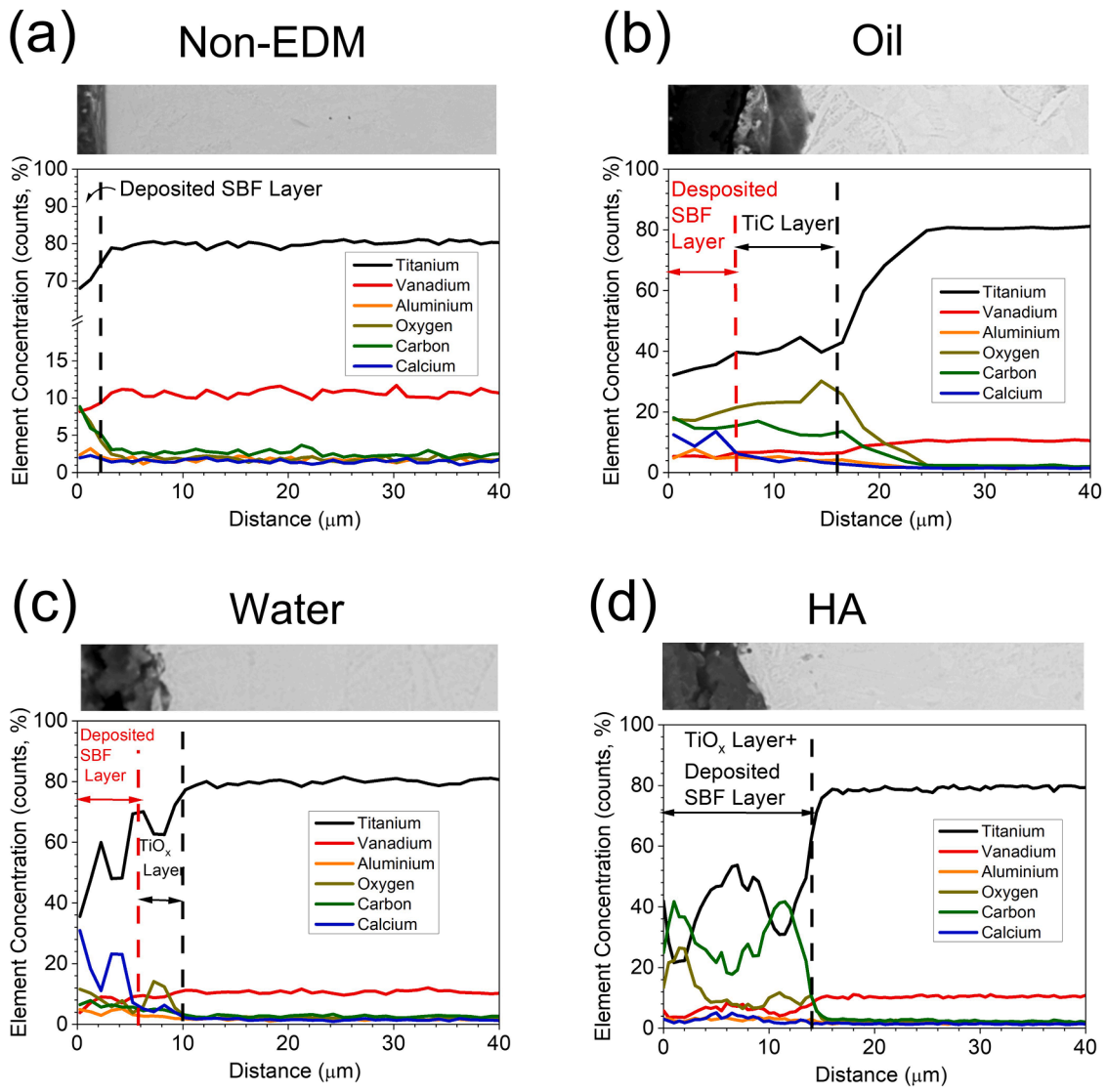

Fig. 14. Depth-dependant EDS analysis (with backscattered electrons) of (a) non-EDMed, (b) oil EDMed, (c) water EDMed, and (d) HA EDMed Ti64 samples after 2352 h of immersion in SBF (pH 7.4, 37.5 °C).

degradation related to the adsorption-desorption process. The evolution of the deposited layer – its deposition, growth, and reduction – significantly influenced the solution resistance (R_s), with deposition and growth increasing R_s and dissolution decreasing it.

The corrosion mechanism evolution for oil-EDMed samples comprised five distinct stages (Fig. 15**(b)**). Initially (2 to 24 h), the dominant processes were TiC interaction and bared material exposure. The high initial surface roughness of the TiC layer (as indicated by low n_{TiC} (≈0.7) [15,34]) likely contributed to the observed fluctuations in layer thickness and decreasing resistance while the layer underwent degradation [32,41]. At 48 h, passive film formation began, likely under the existing TiC layer [4,18]. Fluctuations in passive film thickness and resistance suggest instability, potentially due to limited and variable O access [15]. From 72 to 504 h, SBF deposition created a layer that decreased in resistance while increasing in thickness. This is likely due to imperfections within the layer [15]. The layer's roughness (low n_{de} [16,34] is influenced by the substrate topography [15,54,55]. In the fourth stage (672 to 1512 h), adsorption-desorption processes were observed, and diffusion processes replaced the earlier deposition. Imperfections within the layer likely contributed to the decreased resistance and diffusion impedance [15]. Finally (2352 h), the corrosion mechanism resembled the third stage, but the deposited layer showed improved resistance and reduced roughness. This suggests that re-deposition might have blocked imperfections, hindering diffusion [15] and promoting a more homogeneous layer formation [54,55]. Interestingly, the solution resistance (R_s) evolved similarly to the non-EDMed samples.

The corrosion mechanism of HA-EDMed samples evolved in five stages (Fig. 15**(c)**). Initially (2 h or less), the mechanism mirrored the non-EDMed samples, but the passive film resistance was too high for accurate calculation [58]. Between 24 and 48 h, the passive film resistance decreased and later increased until 336 h. While the passive film thickness remained constant, the roughness increased over time. This suggests that the crack-rich passive film formed during EDM [13,15] gradually sealed, increasing resistance. However, subsequent interaction of Ca and P ions with TiO_x led to local passive film dissolution and decreased resistance [4], also contributing to increased roughness (as indicated by n_f values [16]). From 72 to 504 h, SBF deposition formed a rough layer (n_{de}≈0.7 [20]) influenced by the initial substrate roughness [54,55]. Despite the expected deposition over time, the layer resistance decreased, likely due to localized dissolution by water creating imperfections [13]. Solution resistance (R_s) followed a similar trend to previous cases. The final two stages (4 and 5) mirrored those of non-EDMed samples, likely due to the similar chemical composition of the deposited

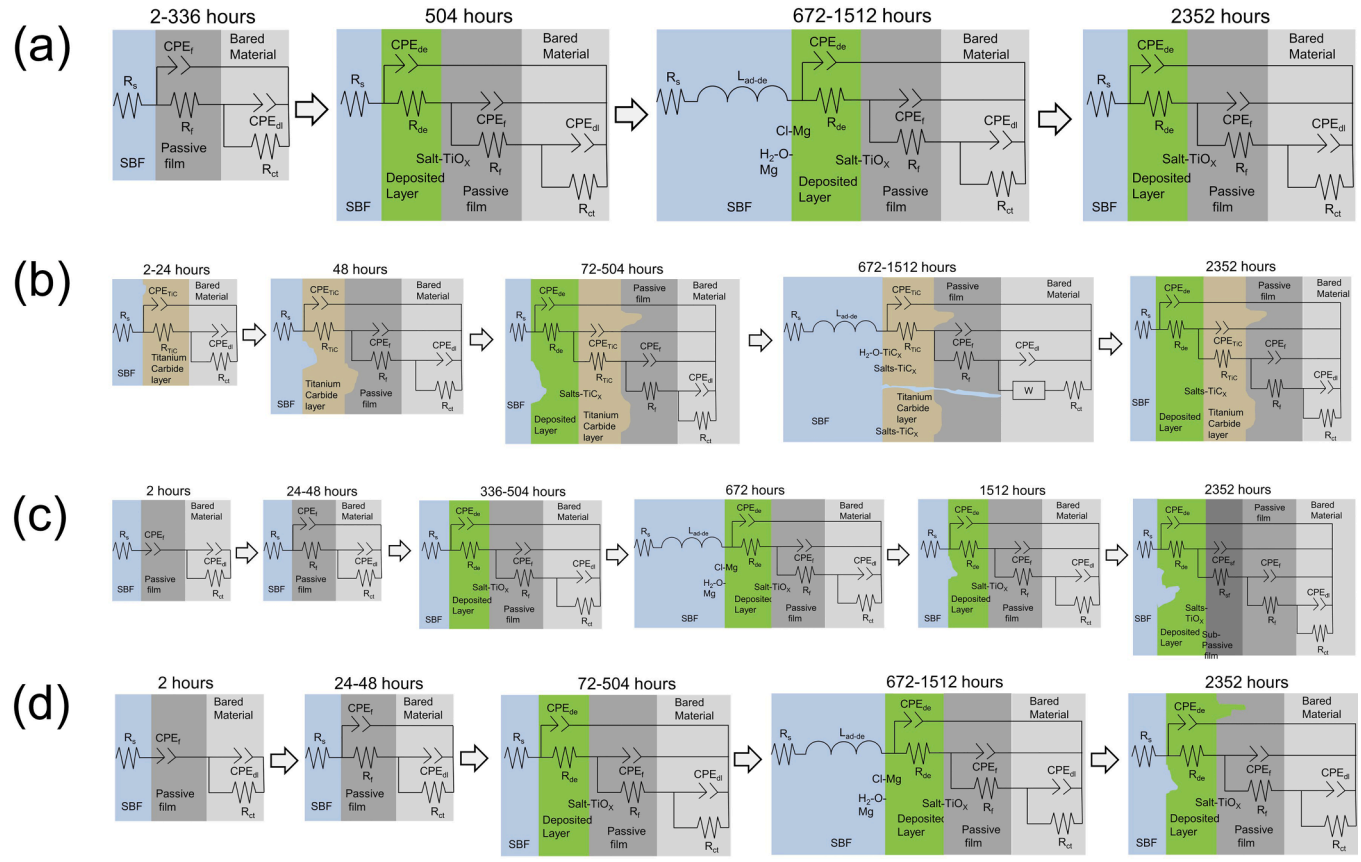

Fig. 15. Corrosion mechanism evolution over the time in SBF immersion for (a) non-EDMed, (b) oil, (c) water, and (d) HA samples.

layers (TiO_x).

Water-EDMed samples exhibited a six-stage corrosion mechanism evolution (Fig. 15**(d)**). The first five stages mirrored those of HA-EDMed samples in terms of corrosion processes, but with differing timeframes (except for the initial 2-hour stage). Specifically, the second stage occurred from 24 to 96 h, the third from 336 to 504 h, the fourth at 672 h, and the fifth at 1512 h. Unlike HA-EDMed samples, the water-EDMed samples' passive film maintained constant thickness and resistance, while surface roughness decreased (increasing n_f). This suggests that the EDM-induced surface relief is gradually reduced due to passive film growth and blockage of defects [4,13,15]. The deposited layer characteristics fluctuated, likely due to cyclical deposition-dissolution and damage-recovery processes [15]. The adsorption-desorption process was observed only at 672 h, indicating the strong influence of substrate topography and chemical composition on the deposited layer. In the final stage (2352 h), a unique mechanism emerged, including a deposited layer, sub-passive film, passive film, and bared material. This formation of a secondary passive film could be due to the high porosity of the original film [13]. Solution resistance (R_s) evolved similarly to previous sample types.

Oil-EDMed samples exhibited a unique corrosion process associated with the distinct TiC layer formed during EDM. This layer's chemical composition differs significantly from the TiO_x-based passive film, making it electrochemically distinguishable [57]. In contrast, the EDM layers on water-EDMed and HA-EDMed samples, also composed of TiO_x, are electrochemically like the native passive film.

While SBF deposition occurred on all sample surfaces, the initiation time varied. Oil-EDMed and HA-EDMed samples showed the shortest deposition times, likely due to the carbon in the TiC layer promoting SBF element adhesion [24], and the presence of HA enhancing deposition on the HA-EDMed samples [22]. Increased surface roughness also encourages deposition by enlarging the contact area [54,55], explaining the faster deposition on water-EDMed samples compared to the smoother non-EDMed samples.

The total resistance of the samples was defined the sum of all resistances (R_f, R_{ct}, R_{de}, R_{TiC} and R_{sf}). This resistance is more or less the same the polarisation resistance (R_p) that in turns is inversely proportional to corrosion current density (I_{corr}) [59], as indicat Eq. (1) [32].

$$I_{corr} = \frac{\beta_a \times \beta_c}{2.303(\beta_a + \beta_c) \times R_p} \quad (1)$$

Where β_a and β_c are the anodic and cathodic slopes, respectively. I_{corr} is proportional to the corrosion rate (*C.R.*), as showing the Eq. (2) [19,48,51].

$$C.R. = \frac{I_{corr} \times M}{e \times F \times \rho} \quad (2)$$

The corrosion rate (C.R.) was calculated using the Faraday equation, where M, e, F, and ρ represent molar mass, number of electrons transferred, Faraday's constant, and material density, respectively. Higher total resistance values signify lower C.R. and, consequently, better corrosion resistance. Fig. 16 depicts the evolution of total resistance over time for each sample type.

All samples initially exhibited an increase in total resistance, likely due to the formation and growth of protective layers (passive film and deposited layer [4]). This initial growth phase varied in duration: shortest for oil and HA-EDMed samples (72 h) and longest for water-EDMed and non-EDMed specimens (96 h). Protective layers with homogeneous chemical compositions generally offer superior corrosion resistance due to the reduced formation of microgalvanic cells [32].

Beyond a certain immersion time, total resistance decreased, indicating a decline in corrosion resistance. This likely stems from localized dissolution of the passive film by anions (Cl^- and SO_4^{-2}), creating imperfections that compromise its integrity [50]. The decline continued

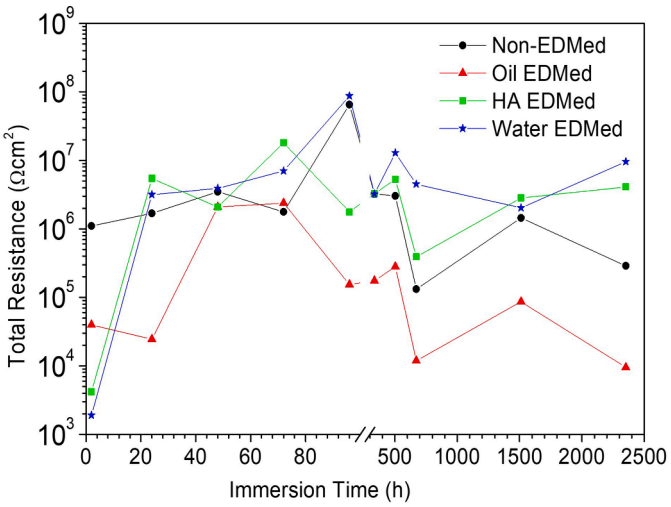

Fig. 16. Evolution of total resistance over immersion time for the tested samples.

until the end of the testing for oil-EDMed and non-EDMed samples. However, water and HA-EDMed samples showed resistance stabilization around 504 and 336 h, respectively, potentially due to the thicker, more stable passive films created by EDM. Note that this effect was absent for oil-EDMed samples, likely due to the heterogeneous chemical composition of the TiC layer promoting microgalvanic corrosion [32].

Samples ranked as follows in terms of overall total resistance: water-EDMed > HA-EDMed > non-EDMed > oil-EDMed. Resistance is known to be proportional to passive film thickness [4], and heterogeneous chemical composition compromises corrosion resistance [32]. While HA adhesion on HA-EDMed samples introduces some heterogeneity, the absence of this effect and the likely thicker passive film explain the superior resistance of water-EDMed samples. The heterogeneous composition of the oil-EDMed samples accounts for their lowest resistance ranking.

5. Conclusion

This study elucidated the long-term corrosion mechanisms of Ti64 samples fabricated via EDM using different bath types in simulated body fluid (SBF). The findings demonstrate that:

(1) Corrosion mechanisms vary significantly based on the EDM bath. While SBF deposition occurs on all surfaces over time, forming a potentially biocompatible protective layer, deposition rates differ. Oil and HA-EDMed samples exhibit the fastest deposition, suggesting enhanced biocompatibility.
(2) Oil-EDMed samples uniquely form a passive film beneath the TiC layer at 48 h, highlighting the layer's permeability. An adsorption-desorption process occurs around 672 h of immersion for most samples, with water-EDMed samples exhibiting an earlier cessation.
(3) Corrosion resistance initially increases for all samples but decreases over time. However, water and HA-EDMed samples demonstrate long-term stabilization, suggesting better corrosion resistance than non-EDMed samples. Oil-EDMed samples exhibit the poorest corrosion resistance, potentially due to their heterogeneous composition.
(4) Despite presenting the highest corrosion resistance, HA-EDMed samples offer greater potential for biomedical implants due to their superior biointegration. This approach provides a cost-effective and efficient route to fabricate Ti64 surfaces with excellent corrosion resistance and biocompatibility, holding significant promise for the biomedical industry.

CRediT authorship contribution statement

J.I. Ahuir-Torres: Writing – original draft, Visualization, Validation, Methodology, Investigation, Formal analysis, Data curation, Conceptualization. **J. Chadwick:** Investigation, Formal analysis, Data curation. **G. West:** Writing – review & editing, Formal analysis. **H.R. Kotadia:** Writing – review & editing, Writing – original draft, Validation, Supervision, Investigation. **T.T. Öpöz:** Writing – review & editing, Writing – original draft, Visualization, Validation, Supervision, Funding acquisition, Conceptualization.

Declaration of competing interest

The authors have no conflicts of interest.

Data availability

Data will be made available on request.

Acknowledgement

This work was partially supported by Liverpool John Moores University, Faculty of Engineering and Technology (FET) Pump Prime Awards 2022/23.

References

[1] P.S. Bains, M. Bahraminasab, S.S. Sidhu, G. Singh, On the machinability and properties of Ti–6Al–4V biomaterial with n-HAp powder–mixed ED machining, Proc. Inst. Mech. Eng., Part H: J. Eng. Med. 234 (2020) 232–242.
[2] G. Singh, T.R. Ablyaz, E.S. Shlykov, K.R. Muratov, A.S. Bhui, S.S. Sidhu, Enhancing corrosion and wear resistance of Ti6Al4V alloy using CNTs mixed electro-discharge process, Micromachines (Basel) 11 (2020) 850.
[3] I. Lavos-Valereto, S. Wolynec, I. Ramires, A.C. Guastaldi, I. Costa, Electrochemical impedance spectroscopy characterization of passive film formed on implant Ti–6Al–7Nb alloy in Hank's solution, J. Mater. Sci.: Mater. Med. 15 (2004) 55–59.
[4] V. Alves, R. Reis, I. Santos, D. Souza, T.d.F. Gonçalves, M. Pereira-da-Silva, A. Rossi, L. Da Silva, In situ impedance spectroscopy study of the electrochemical corrosion of Ti and Ti–6Al–4V in simulated body fluid at 25 C and 37 C, Corros. Sci. 51 (2009) 2473–2482.
[5] M. Hussein, A. Madhan Kumar, A.F. Abdelaal, M. Abdul Azeem, Surface analysis and in vitro corrosion properties in artificial saliva of surface-treated Ti6Al4V alloy for dental applications, Metallur. Mater. Trans. A 52 (2021) 4299–4309.
[6] S. Tamilselvi, V. Raman, N. Rajendran, Corrosion behaviour of Ti–6Al–7Nb and Ti–6Al–4V ELI alloys in the simulated body fluid solution by electrochemical impedance spectroscopy, Electrochim. Acta 52 (2006) 839–846.
[7] B. Sivakumar, S. Kumar, T.S. Narayanan, Fretting corrosion behaviour of Ti–6Al–4V alloy in artificial saliva containing varying concentrations of fluoride ions, Wear. 270 (2011) 317–324.
[8] C.A.R. Maestro, M.C. Ferreira, A.H.S. Bueno, A.M. de Sousa Malafaia, Corrosion resistance of Ti-6Al-4V machined surfaces improved by thermal oxidation, Eng. J. 24 (2020) 185–193.
[9] R.W.-W. Hsu, C.-C. Yang, C.-A. Huang, Y.-S. Chen, Electrochemical corrosion properties of Ti–6Al–4V implant alloy in the biological environment, Mater. Sci. Eng.: A 380 (2004) 100–109.
[10] R. Luo, Z. Liu, F. Yan, Y. Kong, Y. Zhang, The biocompatibility of hydroxyapatite film deposition on micro-arc oxidation Ti6Al4V alloy, Appl. Surf. Sci. 266 (2013) 57–61.
[11] J. Lu, G. Wei, Y. Yu, X. Zhao, Y. Dai, Enhanced corrosion resistance of TA2 titanium via anodic oxidation in mixed acid system, Int. J. Electrochem. Sci. 12 (2017) 2763–2776.
[12] H.R.A. Bidhendi, M. Pouranvari, Corrosion study of metallic biomaterials in simulated body fluid, Metallurg. Mater. Eng. (2012).
[13] E. Matykina, R. Arrabal, B. Mingo, M. Mohedano, A. Pardo, M. Merino, In vitro corrosion performance of PEO coated Ti and Ti6Al4V used for dental and orthopaedic implants, Surf. Coat. Technol. 307 (2016) 1255–1264.
[14] D. Krupa, J. Baszkiewicz, B. Rajchel, A. Barcz, J. Sobczak, A. Biliński, T. Borowski, Effect of calcium-ion implantation on the corrosion resistance and bioactivity of the Ti6Al4V alloy, Vacuum 81 (2007) 1310–1313.
[15] A.A. El Hadad, E. Peón, F.R. García-Galván, V. Barranco, J. Parra, A. Jiménez-Morales, J.C. Galván, Biocompatibility and corrosion protection behaviour of hydroxyapatite sol-gel-derived coatings on Ti6Al4V alloy, Materials (Basel) 10 (2017) 94.
[16] X. Chen, Q. Liao, M. Gong, Q. Fu, Corrosion performances of selective laser melting Ti6Al4V alloy in different solutions, Metals (Basel) 13 (2023) 192.

[17] C. Prakash, M. Uddin, Surface modification of β-phase Ti implant by hydroaxyapatite mixed electric discharge machining to enhance the corrosion resistance and in-vitro bioactivity, Surf. Coat. Technol. 326 (2017) 134–145.
[18] M. Al-Amin, A.M. Abdul-Rani, M. Danish, S. Rubaiee, A.b. Mahfouz, H. M. Thompson, S. Ali, D.R. Unune, M.H. Sulaiman, Investigation of coatings, corrosion and wear characteristics of machined biomaterials through hydroxyapatite mixed-EDM process: a Review, Materials (Basel) 14 (2021) 3597.
[19] A. Mahajan, S. Devgan, S.S. Sidhu, Surface alteration of biomedical alloys by electrical discharge treatment for enhancing the electrochemical corrosion, tribological and biological performances, Surf. Coat. Technol. 405 (2021) 126583.
[20] S.K. Manderna, P. Katyal, M. Gupta, V. Singh, Wear and corrosion Behaviour of wire electrical discharge machined Ti-6A1-4V alloy, in: IOP Conference Series: Materials Science and Engineering, IOP Publishing, 2022 012067.
[21] N. Ekmekci, B. Ekmekci, Electrical discharge machining of Ti6Al4V in hydroxyapatite powder mixed dielectric liquid, Mater. Manuf. Process. 31 (2016) 1663–1670.
[22] O. Tahsin, H. Yasar, M. MURPHY, N. EKMEKCİ, B. EKMEKCİ, Ti6Al4V surface modification by hydroxyapatite powder mixed electrical discharge machining for medical applications, Int. J. Adv. Eng. Pure Sci. 31 (2018) 1–10.
[23] S.-L. Chen, M.-H. Lin, G.-X. Huang, C.-C. Wang, Research of the recast layer on implant surface modified by micro-current electrical discharge machining using deionized water mixed with titanium powder as dielectric solvent, Appl. Surf. Sci. 311 (2014) 47–53.
[24] P. Harcuba, L. Bačáková, J. Stráský, M. Bačáková, K. Novotna, M. Janeček, Surface treatment by electric discharge machining of Ti–6Al–4V alloy for potential application in orthopaedics, J. Mech. Behav. Biomed. Mater. 7 (2012) 96–105.
[25] F. Otsuka, Y. Kataoka, T. Miyazaki, Enhanced osteoblast response to electrical discharge machining surface, Dent. Mater. J. 31 (2012) 309–315.
[26] T. Chang-bin, L. Dao-Xin, W. Zhan, G. Yang, Electro-spark alloying using graphite electrode on titanium alloy surface for biomedical applications, Appl. Surf. Sci. 257 (2011) 6364–6371.
[27] B. Ekmekci, Residual stresses and white layer in electric discharge machining (EDM), Appl. Surf. Sci. 253 (2007) 9234–9240.
[28] K. Dhakar, R. Kumar, A. Katheria, L. Nagdeve, H. Kumar, Effect of various dielectric fluids on electric discharge machining (EDM): a review, J. Brazil. Soc. Mech. Sci. Eng. 44 (2022) 487.
[29] A. Pramanik, A. Basak, G. Littlefair, S. Debnath, C. Prakash, M.A. Singh, D. Marla, R.K. Singh, Methods and variables in Electrical discharge machining of titanium alloy–a review, Heliyon. 6 (2020).
[30] B. Ekmekci, Y. Ersöz, How suspended particles affect surface morphology in powder mixed electrical discharge machining (PMEDM), Metallur. Mater. Trans. B 43 (2012) 1138–1148.
[31] T.T. Öpöz, H. Yaşar, N. Ekmekci, B. Ekmekci, Particle migration and surface modification on Ti6Al4V in SiC powder mixed electrical discharge machining, J. Manuf. Process. 31 (2018) 744–758.
[32] J. Ahuir-Torres, H. Kotadia, T. Öpöz, Effect of the electrical discharge machining on Ti6Al4V corrosion behaviour in simulated body fluid, Surf/ Coat. Technol. 470 (2023) 129830.
[33] Y. Sasikumar, M. Solomon, L. Olasunkanmi, E. Ebenso, Effect of surface treatment on the bioactivity and electrochemical behavior of magnesium alloys in simulated body fluid, Mater. Corros. 68 (2017) 776–790.
[34] C. Liu, Q. Bi, A. Leyland, A. Matthews, An electrochemical impedance spectroscopy study of the corrosion behaviour of PVD coated steels in 0.5 N NaCl aqueous solution: part II, EIS Interpret. Corros. Behav., Corros. Sci. 45 (2003) 1257–1273.
[35] B. Ekmekci, White layer composition, heat treatment, and crack formation in electric discharge machining process, Metallurg. Mater. Trans. B 40 (2009) 70–81.
[36] H. Rahimi, S. Masoudi, M. Tolouei-Rad, Experimental investigation of the effect of EDM parameters and dielectric type on the surface integrity and topography, Int. J. Adv. Manuf. Technol. 118 (2022) 1767–1778.
[37] E. McCafferty, Introduction to Corrosion Science, Springer Science & Business Media2010.
[38] I.-J. Hwang, H.-C. Choe, W.A. Brantley, Electrochemical characteristics of Ti-6Al-4V after plasma electrolytic oxidation in solutions containing Ca, P, and Zn ions, Surface and Coatings Technology 320 (2017) 458–466.
[39] K. Leksycki, A. Kaczmarek-Pawelska, K. Ochał, A. Gradzik, D.Y. Pimenov, K. Giasin, D. Chuchala, S. Wojciechowski, Corrosion resistance and surface bioactivity of Ti6Al4V alloy after finish turning under ecological cutting conditions, Materials (Basel) 14 (2021) 6917.
[40] S.L. de Assis, S. Wolynec, I. Costa, Corrosion characterization of titanium alloys by electrochemical techniques, Electrochim. Acta 51 (2006) 1815–1819.
[41] J.C. Grotberg, Modifying Ti6Al4V Implant Surfaces: Cell Responses and Corrosion Resistance of Annealed Titania Nanotubes, University of Illinois at Chicago, 2014.
[42] F. Ciucci, Modeling electrochemical impedance spectroscopy, Curr. Opin. Electrochem. 13 (2019) 132–139.
[43] Q. Liu, M. Chen, Y. Yang, The effect of chloride ions on the electrochemical dissolution of chalcopyrite in sulfuric acid solutions, Electrochim. Acta 253 (2017) 257–267.
[44] D.A. Harrington, P. Van Den Driessche, Mechanism and equivalent circuits in electrochemical impedance spectroscopy, Electrochim. Acta 56 (2011) 8005–8013.
[45] H.S. Magar, R.Y. Hassan, A. Mulchandani, Electrochemical impedance spectroscopy (EIS): principles, construction, and biosensing applications, Sensors 21 (2021) 6578.
[46] J. Navarro-Laboulais, J. García-Jareño, F. Vicente, Kramers–Kronig transformation, dc behaviour and steady state response of the Warburg impedance for a disk electrode inlaid in an insulating surface, J. Electroanal. Chem. 536 (2002) 11–18.
[47] M.V. Diamanti, F. Bolzoni, M. Ormellese, E. Pérez-Rosales, M. Pedeferri, Characterisation of titanium oxide films by potentiodynamic polarisation and electrochemical impedance spectroscopy, Corros. Eng. Sci. Technol. 45 (2010) 428–434.
[48] L.-Y. Chen, H.-Y. Zhang, C. Zheng, H.-Y. Yang, P. Qin, C. Zhao, S. Lu, S.-X. Liang, L. Chai, L.-C. Zhang, Corrosion behavior and characteristics of passive films of laser powder bed fusion produced Ti–6Al–4V in dynamic Hank's solution, Mater. Des. 208 (2021) 109907.
[49] G. Yi, X. Liu, C. Zheng, H. Zhang, C. Xu, Y.-W. Cui, S. Liu, Characteristics of passive films formed on As-Cast Ti–6Al-4V in Hank's solution before and after transpassivation, Front. Mater. 7 (2021) 640081.
[50] M. Metikos-Huković, A. Kwokal, J. Piljac, The influence of niobium and vanadium on passivity of titanium-based implants in physiological solution, Biomaterials 24 (2003) 3765–3775.
[51] Z. Wen, C. Wu, C. Dai, F. Yang, Corrosion behaviors of Mg and its alloys with different Al contents in a modified simulated body fluid, J. Alloys Compd. 488 (2009) 392–399.
[52] A.L.R. Ribeiro, P. Hammer, L.G. Vaz, L.A. Rocha, Are new TiNbZr alloys potential substitutes of the Ti6Al4V alloy for dental applications? An electrochemical corrosion study, Biomed. Mater. 8 (2013) 065005.
[53] J. Bonkerud, C. Zimmermann, P.M. Weiser, L. Vines, E.V. Monakhov, On the permittivity of titanium dioxide, Sci/ Rep. 11 (2021) 12443.
[54] Y. Ammar, D. Swailes, B. Bridgens, J. Chen, Influence of surface roughness on the initial formation of biofilm, Surf. Coat. Technol. 284 (2015) 410–416.
[55] S. Kumar, G. Bae, C. Lee, Influence of substrate roughness on bonding mechanism in cold spray, Surf. Coat. Technol. 304 (2016) 592–605.
[56] U. Retter, H. Lohse, Electrochemical impedance spectroscopy. Electroanalytical Methods: Guide to Experiments and Applications, Springer, 2009, pp. 159–177.
[57] B.F. Mohazzab, B. Jaleh, A. Fattah-alhosseini, F. Mahmoudi, A. Momeni, Laser surface treatment of pure titanium: microstructural analysis, wear properties, and corrosion behavior of titanium carbide coatings in Hank's physiological solution, Surf. Interfaces. 20 (2020) 100597.
[58] J.I. Ahuir-Torres, J. Hernández-López, M. Arenas, A. Conde, J. De Damborenea, Synthesis of TiO2 nanopore arrays by pulsed laser treatment and anodic oxidation, Surf. Coat. Technol. 259 (2014) 408–414.
[59] M. Stern, A.L. Geary, Electrochemical polarization: I. A theoretical analysis of the shape of polarization curves, J. Electrochem. Soc. 104 (1957) 56.